MASTERARBEIT

Titel der Masterarbeit

„Quantification of Metal-Phytosiderophore complexes via LC-ICP-MS"

verfasst von

Anna Regelsberger, B.Sc.

angestrebter akademischer Grad

Master of Science (MSc)

Wien, 2015

Studienkennzahl lt. Studienblatt: A 066 862
Studienrichtung lt. Studienblatt: Masterstudium Chemie

Betreut von: ao. Univ.-Prof. Mag. Dr. Regina Krachler

Acknowledgments

I would like to thank ao. Univ.-Prof. Dr. Regina Krachler for the supervision of this work and assoc. Prof. Dr. Stephan Hann for his guidance over the course of it.

Many thanks also to my colleagues in the working group of the Division of Analytical Chemistry at the BOKU for their help and providing a great working atmosphere.

Finally, I offer my thanks to my family, for their support and motivation during the long process of finalising my thesis.

Index

1. Introduction

1.1.   General

Iron is an essential trace element for most organisms and its absence causes deficiency symptoms – iron chlorosis in plants. But while the iron present in soils is generally sufficient, the low solubility of iron oxides formed under oxic conditions can cause iron deficiencies in plants. Especially in calcareous soils the amount of Fe(III) ions available can be insufficient for plant growth, as the solubility of Fe(III) ions at pH 4 decreases approximately to one thousandth for each rise in the pH value[1].

Therefore plants have developed different strategies to increase the bioavailability of iron, which can roughly be divided in "strategy I" and "strategy II" mechanisms. While "strategy I" includes the exudation of reducing compounds and small organic acids facilitating iron solubility through acidification of the rhizosphere[2] (the part of the soil interacting with the plant roots) and reducing agents for the uptake of Fe(II), "strategy II" plants have developed organic ligands which are able to form a soluble complex with iron(III). These organic substances, called phytosiderophores (PS; en. *iron carrier*), are synthesized and exuded into the soil by graminaceous plants, including many important crop plants, in case of iron scarceness. The uptake of iron then occurs in form of iron(III)-phytosiderophore-complexes via special transporters.

Phytosiderophores increase the bioavailability of iron in the rhizosphere, as the iron-phytosiderophore complexes become the dominant soluble iron species in calcareous soils. Their concentrations in the rhizosphere are determined by exudation and degradation rates, diffusion away from the roots and advective transport to the root.[3] As diffusion and therefore

concentration gradients play an important role in the iron shuttling by phytosiderophores, a better understanding of the concentrations present in the rhizosphere would be desirable. Due to the complexity of soil matrices as well as the difficulty in sampling, little is known about the fate of phytosiderophores in the soil.

The FWF project "*The rhizosphere biogeochemistry of phytosiderophores and plant iron uptake*", a collaboration between the Department of Environmental Geosciences from the University of Vienna, the Institute of Soil Science and the divisions of Analytical and Organic Chemistry from the University of Natural Resources and Applied Life Sciences Vienna (BOKU), aims to increase that knowledge by studying 2'-deoxymugineic acid (DMA) in soil matrices from several perspectives: the synthesis of DMA, the development of sensitive analytical methods for phytosiderophores and their metal complexes, and the investigation of phytosiderophore concentrations in the rhizosphere, their susceptibility to soil adsorption, degradation, changes in soil pH or redox potential, phytosiderophore-promoted iron mobilisation and uptake mechanisms. The collected information will be used to develop a rhizosphere reactive transport model quantitatively evaluating the importance of processes connected to iron acquisition in strategy II plants.

As part of the analytical aspect of the project, the objective of this thesis is testing the suitability of a new analytical method to measure metal phytosiderophore complexes in soil matrices.

1.2.   Mugineic acids (MAs)

Mugineic acids (MAs) are a group of common phytosiderophores, including 2'-deoxymugineic acid (DMA), mugineic acid (MA) and hydroxymugineic acid (HMA) as well as their respective enantiomeres 2'-epi-MA and 3'-epi-HMA. Their chemical structures are very similar, the only difference being the (non-)existence of two hydroxyl-groups (R_1 and R_2, see Figure 1).
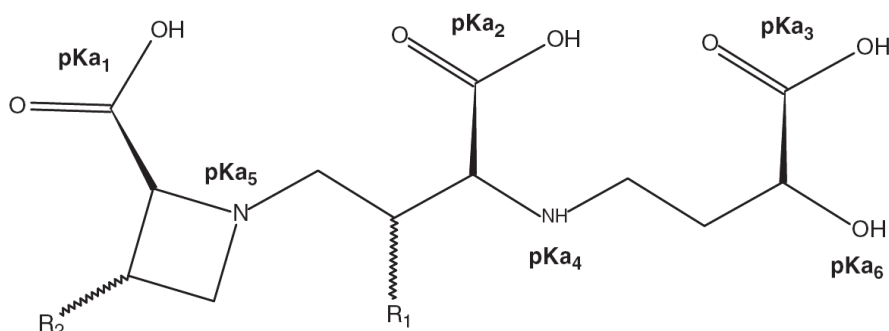
Figure 1: Mugineic acids (MAs)

Mugineic acid (MA), hydroxymugineic acid (HMA) and 2'-Deoxymugineic acid (DMA) only differ in their hydroxylation pattern. MA: $R_1 = \alpha\text{-OH}$, $R_2 = H$; 2'-DMA: $R_1 = R_2 = H$; HMA: $R_1 = R_2 = \alpha\text{-OH}$; 3-epi-HMA and 2'-epi-MA: $R_1 = \beta\text{-OH}$.[4]

Plants synthesize those nonproteinaceous amino acids from nicotianamine by transamination and hydroxylation to DMA, or with further hydroxylation to MA and HMA.[5]

As the MA with the fewest hydroxylation groups, DMA ($C_{12}N_2O_7H_{20}$) has a molecular weight of 304 g mol^{-1}. Its ammonia salt weights 321.33 g mol^{-1}.

Mugineic acids are zwitterionic. Under neutral conditions, DMA possesses three deprotonated carboxy-groups, while the hydroxyl- and the two amino groups are protonated, as can be determined from the pK_a values shown in Table 1.[6] In total, the compound is thereby singly negatively charged (see Figure 2) which can be notated as [DMA-H]$^-$.

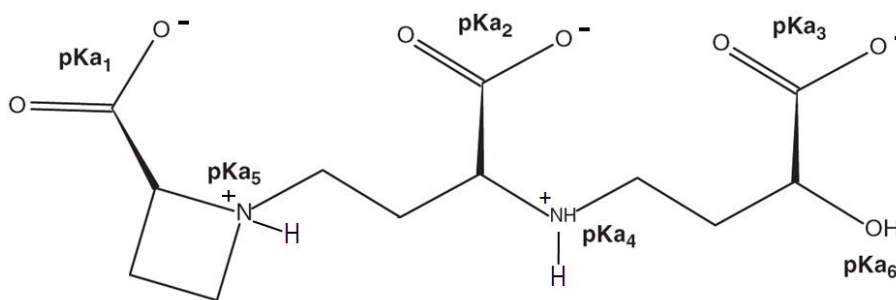| $pK_{a,1}$	$pK_{a,2}$	$pK_{a,3}$	$pK_{a,4}$	$pK_{a,5}$	$pK_{a,6}$
2.35	2.74	3.20	8.25	10.00	17.1

Table 1: pK_a values of DMA[6]

Figure 2: DMA under neutral conditions

Under neutral conditions (pH 6.5), DMA is zwitterionic and in total singly negatively charged, as can be seen from its pKa-values (see Table 1).

1.2.1. *Metal complexes with mugineic acids*

Phytosiderophores of the mugineic acid group form hexadentate complexes in a nearly octahedral shape with bivalent and trivalent metals. The stereoscopic drawing of a MA-Co(III) complex shown in Figure 3 was determined by X-ray crystallographic analysis and confirmed through ^{1}H NMR spectra for the complex structures in aqueous solution by Sugiura and Nomoto (1984). DMA complexes are formed analogically. As can be seen, the phytosiderophores bind with the azetidine ring nitrogen, the secondary amine nitrogen, all three carboxylate oxygens as well as the terminal hydroxyl oxygen[2].

According to Murukami et al. (1989), the metal complexes are singly negatively charged with both bivalent and trivalent metals under neutral conditions, as the α-hydroxyl-group is protonated accordingly. Due to the higher charge density of trivalent metal cations, the hydroxyl-group dissociates in complexes with Co(III) and Fe(III) (see Figure 3)[4, 6]. While Murukami et al. (1989) observed neutral phytosiderophore complexes at pH 4 and lower, von Wirén et al. (2000) suggested that DMA partially dissociates to a neutral tetradentate Fe complex even at pH 7 and the neutral species predominates at pH 6 and lower[6]. Kraemer et al. (2006) discount the associated stability constant, as it underpredicted the dissolvated iron concentrations at pH 7 and 8 observed in several studies[3].
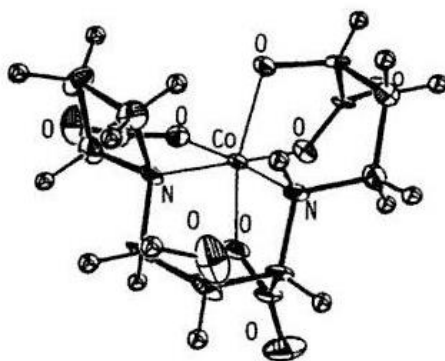
Figure 3: Co(III)-MA complex

Phytosiderophores of the mugineic acid group form hexadentate octahedral metal complexes with bivalent and trivalent metals. The stereoscopic drawing of a Co(III)-MA complex shown was determined by X-ray crystallographic analysis[2].

MAs have a much smaller affinity for iron(III) than microbial siderophores. While calcium, magnesium and aluminium – three metals often present in high concentrations in soils – compete only minimally with iron for chelation, several transition metals as well as zinc and arsenic have been suggested as possible central atoms for metal complexes with mugineic acids. Phytosiderophores are therefore considered to play a role in plant uptake of micronutrients such as zinc and copper as well as in the mobilization of heavy metals, for instance cadmium or arsenic.

The importance of the different metal-phytosiderophore complexes is much discussed, as contradictory observations have been made. While it is known that MAs form stable complexes with several metals and competing Cu and Zn lower the solubility of iron solutions, iron mobilization in calcareous soils is less affected. This could be explained by the fact that contrary to iron, soluble Cu concentrations are not controlled by solubility equilibria, but by adsorption and complexation processes.[3]

The Irving-Williams sequence in the order of $Ca^{2+} < Mn^{2+} < Fe^{2+} < Co^{2+} < Ni^{2+} < Cu^{2+} > Zn^{2+}$ is followed by metal complexes of MAs[3, 4].

Due to a higher crystal field stabilisation, the Co(III) complex of MA is more stable than the high-spin Fe(III) complex and was therefore proposed as a model for studies on the ferric complex by Sugiura and Nomoto (1984)[2].

1.3. Analysis

To measure natural complexing ligands such as phytosiderophores and their metal complexes in soil matrices, a method is needed that enables speciation, sensitive enough to detect low concentrations as present in the soil, and robust enough to endure soil matrices. Possible solutions which have been applied to the separation of phytosiderophores are capillary electrophoresis (CE)[6, 10, 11, 19] and high-performance liquid chromatography (HPLC)[10, 11] coupled to a sensitive detection system. So far, the detection methodologies used include atomic absorption spectrometry[7], pulsed amperometric detection[8], post-column derivatisation followed by photometric or fluorimetric detection[9], and mass spectrometry, using electrospray or inductively coupled plasma ionisation[10, 11].

In most cases, HPLC is used for separation. Among the employed principles are size exclusion chromatography, the common cation or anion exchange, ion-pair chromatography, hydrophilic interaction liquid chromatography (HILIC), as well as graphic carbon[12] and mixed mode columns[14].

In order to be able to analyse metal complexes, certain characteristics such as high complex stability and low exchange kinetics are necessary. But analysing non-covalent metal complexes is challenging even if those conditions are satisfied, as the complexes are in equilibrium with their free components and therefore sensitive to pH-changes, trace metal impurities, temperature, etc.

Iron-phytosiderophore complexes pose an additional challenge, as the complex is most stable at a pH-range where iron is hardly soluble – which is easily understandable when considering that they are used by plants to increase the bioavailability of iron in soil (see Chapter 1.1).

To avoid biased errors, decomposition and formation of the complex has to be prevented or controlled during sample storage, preparation and the analysis itself.

Previous studies have shown that the metal complexes of MAs have a high thermodynamic stability and can be separated from their metal complexes via capillary electrophoresis and liquid chromatography, demonstrating that the exchange kinetics are low enough to enable a separation[13, 14].
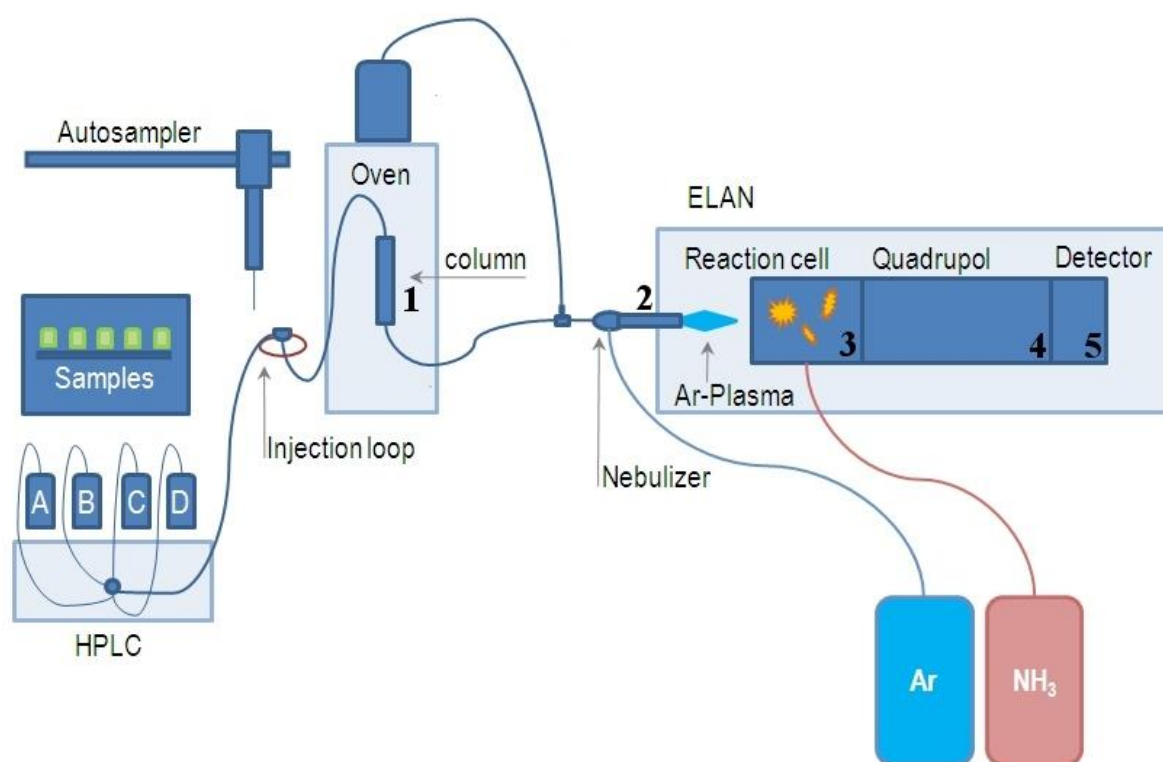

Figure 4: Schematic diagram of a LC-MS system
1. Chromatographic separation; 2. Ionisation; 3. Dynamic Reaction Cell; 4. Mass separation; 5. Detector

The PS complexes are separated chromato-graphically in a mixed mode reversed-phase/weak anion exchange (RP/WAX) column (Figure 4/1.), a slightly adapted LC-ESI-MS/MS method already described by Dell'mour et al. (2012)[14]. N-(10-undecenoyl)-3-amino-quinuclidine selector (pKa ~
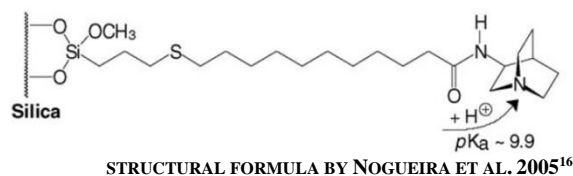
Figure 5: RP/WAX column – functional group

The stationary phase consists of a (N-(10-undecenoyl)-3-aminoquinuclidine selector) covalently immobilized on thiol-modified silica particles (5 µm, 100 Å pore diameter) by radical addition reaction[16].

9.9) is used as a weak anion exchanger at neutral or acidic conditions (see Figure 5). As the PS metal complexes are singly negatively charged under neutral conditions, the main mechanism controlling the separation at pH 6.5 is the anion exchange function of the protonated tertiary amine, where an acetate (Ac^-) or hydroxide (OH^-) is exchanged with the singly negatively charged complex. Hydrophobic interaction with the carbohydrate chain should play only a minor role, as the mugineic acid phytosiderophores are quite polar. Soluble free metals are eluted within the void volume.

ICP Quartz torch

Aerosol (Nebulised Liquid + Ar)

$Ar + e^- \rightarrow Ar^+ + 2e^-$

~5000-8000 K

Load coil: radio frequency

Auxiliary gas   Coolant gas

Electronic ionisation: $M + e^- \rightarrow M^+ + 2e^-$
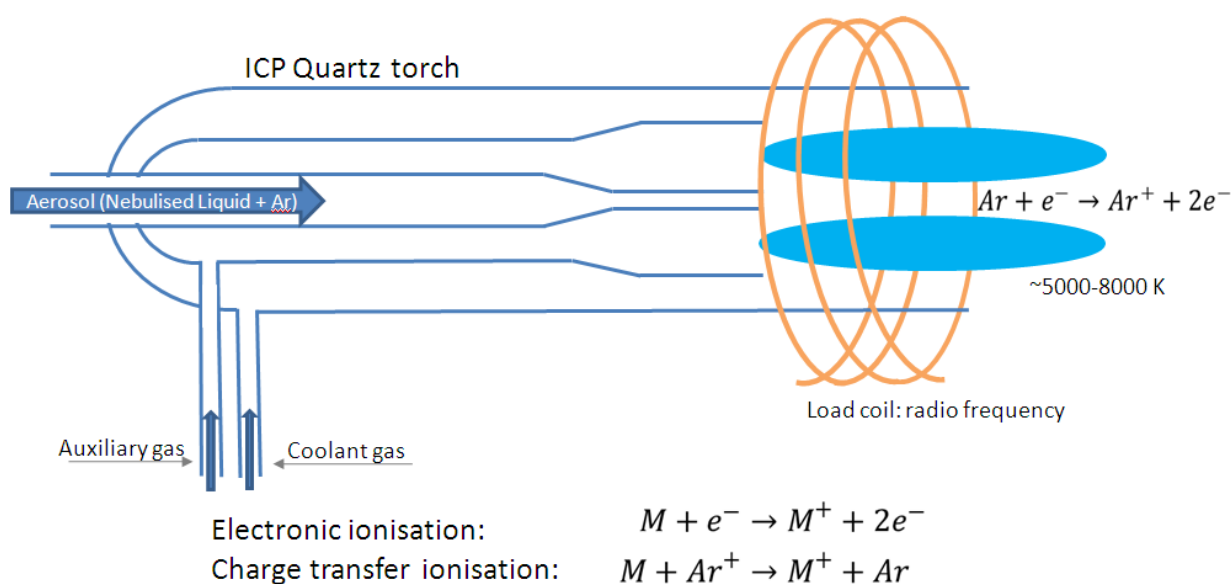Charge transfer ionisation: $M + Ar^+ \rightarrow M^+ + Ar$

Figure 6: ICP torch

Schematic diagram of an inductively coupled plasma (ICP) torch

The separated substances form an aerosol when passing the nebulizer (Figure 4/2.), which is then further transferred into the inductively coupled Argon plasma (Figure 4/3. and Figure 5).

As the argon plasma reaches temperatures of over 5000 K, desolvation, atomization, and finally ionisation takes place. The plasma is operated under atmospheric pressure and produces high backgrounds for H, C, N and O.

Dynamic reaction cell technique reduces interferences with metal hydrides and oxides by introducing a reaction gas – in our case NH_3 – into the cell at an optimised gas flow, resulting in collisions and reactions between the molecules and ions in the gas phase, which leads to interference discharge or dissociation. In the analyzer quadrupole, consisting of four metallic rods, the ions are separated according to their mass-to-charge ratio (m/z) by a combination of direct current and radio frequency fields, allowing only one selected m/z to reach the detector, where the ion will be converted into an electrical pulse. When several isotopes are analysed, the quadrupole switches between different rf-dc voltages for each m/z. The time one m/z is detected is called the dwell time[15].

2. Experimental

2.1.   Chemicals

All water used for sample preparation and LC-ICP-MS measurements was prepared by sub-boiling distillation of purified water (18.2 MΩ) received from an ultra clear unit (SG Wasseraufbereitung und Regenerierstation GmbH, Barsbüttel, Germany). Ammonium hydroxide NH_4OH (25 % ammonia solution, suprapur®), acetic acid AcH (glacial, 100 % suprapur®) and formic acid HCOOH (98-100 % suprapur®) were purchased from Merck KGaA, Darmstadt, Germany, while Methanol (Optima® LC/MS Grade) was obtained from Thermofisher, Fisher Scientific UK Limited, Loughborough, UK).

Metal chlorides used in PS-metal complexes were purchased in trace metal basis from Sigma-Aldrich Co., St. Louis, MO, USA (99.9 % $FeCl_3$, 99.99 % $NiCl_2$, 99.999 % $CoCl_2$, $\geq$99.995 % $CuCl_2$, 99.999 % $ZnCl_2$).

The ammonium salt of 2'-deoxymugineic acid (DMA-NH_4) was synthesized in house with a purity of >95 % by the Division of Organic Chemistry.

Subboiled HNO_3 prepared by a double sub-boiling distillation of 65 % nitric acid p.a. from Merck applying a duoPUR quartz sub-boiling system (MLS Lab Systems GmbH, Leutkirch, Germany) was used in post-column acidification and to stabilize metal spikes such as ^{57}Fe (Chemotrade, 95.48 % enrichment, metallic form) or Indium (1000 ppm Standard).

As cell gas, ammonia (NH_3) from Linde Gas GmbH, Stadl-Paura, Austria (99.999 pure) was used.

As glass always contains metal impurities, all glassware was avoided in sample and eluent preparation and storage.

2.2. Instrumental

A Rheos 2000 Pump from Flux instruments AG, Reinach BL, Switzerland/Thermo Scientific (a quaternary HPLC pump with a low pressure mixing device) with an integrated vacuum degasser Rheos CPS-LC was applied for chromatography and operated via the Rheos 2000 Janeiro II control software. Three channels were used for gradient elution (see Chapter 2.3.2.1 and Chapter 2.3.2.2) at a flow rate set to 250 µL per minute. For separation a 50 x 2 mm PEEK column packed with a mixed mode RP/WAX stationary phase developed by Nogueira et al.[16] was used. The stationary phase consists of a N-(10-undecenoyl)-3-aminoquinuclidine selector (pKa ~ 9.9) covalently immobilized on thiol-modified silica particles (5 µm, 100 Å pore diameter) by radical addition reaction[16]. The column was packed by VDS optilab, Berlin, Germany.

The column was placed in a Mistral oven from Spark Holland B.V., Emmen, The Netherlands, set to 40 °C and connected with a Thermo Scientific PAL autosampler (CTC Analytics AG, Zwingen, Switzerland), operated via the PAL Cycle Composer Version 1.5.4.. The parameters set for the autosampler are listed in Table 2.

Parameters	Settings	Notes
Filling Speed	5 µL s^{-1}	sample & wash solution
Injection Speed	20 µL s^{-1}	sample & wash solution
Filling Strokes	1	
Cleaning	2 x with water, 2 x valve clean	
Post Injection Delay	500 ms	

Table 2: Autosampler settings

The Autosampler was operated via PAL- Cycle Composer Version 1.5.4.. For injection, a 100 µL Hamilton needle was used.

Sample vials were stored in the included stack cooler at 5 °C. For injection a 100 µL Hamilton needle was used. The injection volume was set to 5 µL (loop length).

For analysis, the HPLC was connected with a PFA-nebulizer, creating the aerosol for the Quadrupole ICP-MS detection carried out with an ELAN® ICP-MS systems from PerkinElmer Inc., Waltham, MA 02451 USA in dynamic reaction mode, using ammonia as cell gas at a flow rate of 0.8 mL per minute. The dwell time was set at 50 ms for Fe-56, Fe-57, Co-59, Ni-60 and Zn-66, resulting in 1.25 data points per second. For instrument control/tuning a multi-elemental standard (Stock-ELAN-Tune-Mix with 5 µg/L Li, Mg, Cu, In, Ce, Pb, V and Ba in 5 % HNO_3) was used. Data evaluation was performed with Dionex software Chromeleon 6.80.

For post column spiking and acidification, an Intelligent Pump Al-12-01 (1 mL, PEEK) from Flom Corporation, Tokyo, Japan, was used.

2.3. Methods

2.3.1. Sample preparation

To avoid changes in complex equilibria as far as possible, sample preparation was minimized. The samples were stored at -20 °C, thawed immediately before analysis, diluted with subboiled water when necessary (1:3 or 1:4) and kept at 5 °C in a cooling stack during the measurement.

Standards were prepared by weighing in amounts of 1-15 mg metal chlorides as well as DMA and dissolving each of them in subboiled water the day of the measurement, creating millimolar solutions (25-60 mM). The preparation of 1:1 single-metal-DMA standards was done by adding equimolar amounts of DMA-solution and Metal-solution, while DMA was added in excess for multi-elemental DMA-standards ($c_{DMA} = 6 * c_{Me} = 1,2 * c_{Me,tot}$) to ensure quantitative complexation of all competing metals. Metal concentrations in multi-elemental standards were chosen to fit concentration ranges found in soil samples ($c_{Fe} = 2\ c_{Cu} = 2\ c_{Zn} = 4\ c_{Co} = 4\ c_{Ni}$), with a range from 1 to 20 µM for iron.

Eluent solutions were controlled before the measurement and freshly prepared if necessary. The 100 mM ammonium acetate buffer (NH_4Ac) was prepared by adding 2.87 mL acetic acid to 500 mL water and then adjusting the pH to 6.5 with NH_4OH 25 %.[13]
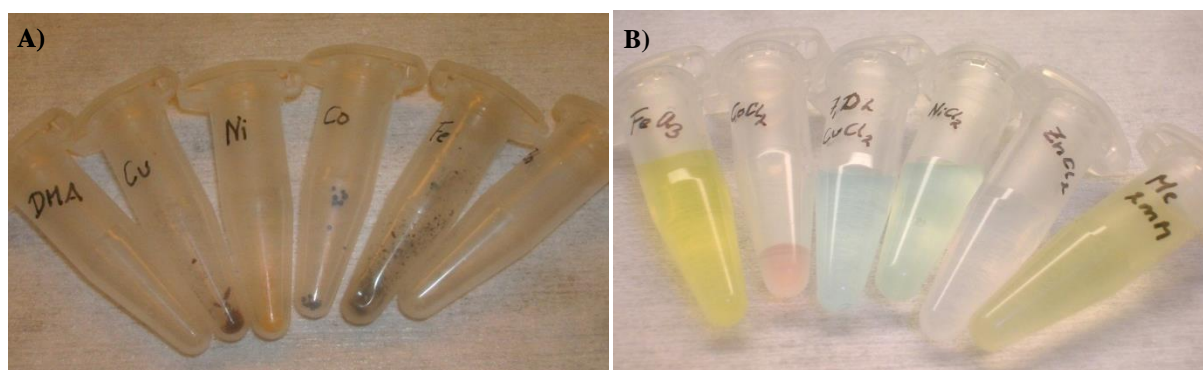

Figure 7: Preparing external standards

The different metal chlorides and DMA were prepared directly before the measurement. A) DMA-NH₄ and the metal chlorides ready for dilution; B) the prepared stock solutions.

2.3.2. Measurements

2.3.2.1. FIA-ICP-MS

To measure the metal concentrations, the samples were analysed via flow injection analysis (FIA) with a flow rate of 250 µL min^{-1} with a constant solvent composition of 50 % v/v H_2O (A), 49 % v/v 100 mM NH_4Ac, pH 6.5 (B) and 1 % v/v Methanol (C), leading to a measurement time of 3 minutes. The injection volume was 5 µL.

Due to iron losses observed at a pH of 6.5 in the LC and the FIA measurement, a FIA-measurement (FIA H^+) with 1 % v/v HCOOH and 48 % v/v ammonia acetate buffer, while all other parameters remained unchanged, was added.
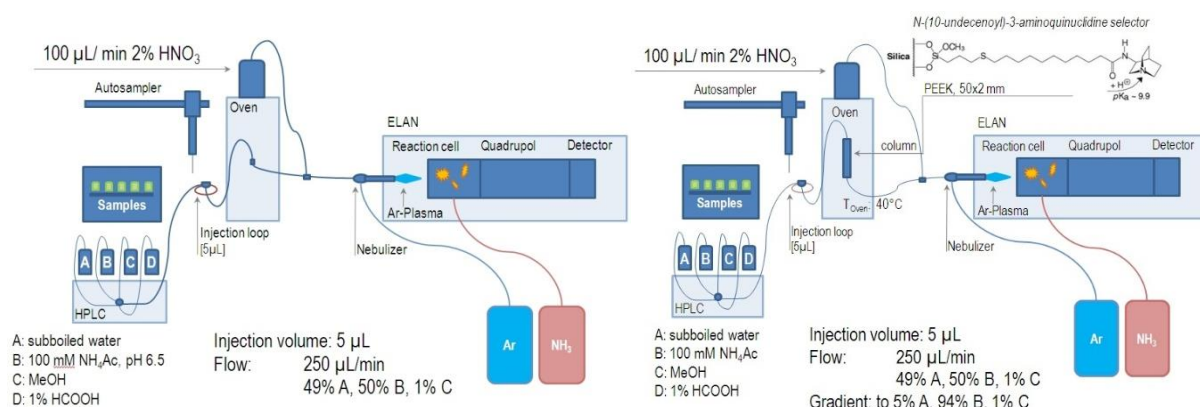

Figure 8: A) FIA-ICP-MS, B) LC-ICP-MS

Schematic diagram of the conditions used for a) FIA-ICP-MS b) LC-ICP-MS

2.3.2.2. LC-ICP-MS

To measure the DMA-complexes, the RP/WAX column (50 x 2 mm PEEK, *N-(10-undecenoyl)-3-aminoquinuclidine selector*)[16] at 40 °C was used for separation at a flow of 250 µL min^{-1}. The solvent composition started with 50 % v/v H_2O, 49 % v/v 100 mM NH_4Ac, pH 6.5 and 1 % v/v Methanol. Methanol was kept constant, while the buffer concentration changed with

time to 94 % v/v (see Table 3). The method was adapted from the LC-ESI-MS/MS method described by Dell'mour et al. (2012)[14].

time / min	H$_2$O / % v/v	NH$_4$Ac / % v/v	Methanol / % v/v	Graph
0	50	49	1	
2.95	50	49	1	
5.25	5	94	1	
5.45	50	49	1	
10	50	49	1	

Table 3: Chromatographic gradient

2.3.2.3. *LC with online IDMS*

Post column isotope dilution MS (IDMS) using ^{57}Fe was applied to quantify the Fe-DMA complexes. ^{57}Fe in 1 % HCl was added with a flow rate of 50 µL min^{-1} to the LC eluent post-column. As a species unspecific standard with a known constant mass flow $M_{spike}(t)$, the iron concentration in the sample c_{sample} can be calculated over isotope ratio changes (illustrated in Figure 9) between ^{57}Fe and ^{56}Fe using Equation 1[17, 18].

$$M_{sample}(t) = M_{Spike}(t) * \frac{R_{spike} - R_{blend}(t)}{R_{blend}(t) - R_{nat}} * \frac{a_{57,spike}}{a_{57,nat}}$$

Equation 1

The IDMS equation allows the calculation of the sample mass flow M_{sample} via R_{blend}, the ratio of the measured values of the two isotopes used. The mass flow of the spike solution M_{spike}, the isotopic ratios in the sample ($R_{sample} = R_{nat}$, see Equation 2) and in the spike (R_{spike}), as well as the isotopic abundances in the sample and in the spike (a_{spike} and a_{nat}) can be considered constant.

This is possible, if the isotopic ratio in the sample can be considered identical with the natural isotopic ratio. If that is the case, the sample mass flow over time $M_{sample}(t)$ and the isotopic ratio of the blend between eluent, sample and spike R_{blend} are the only variables not known, as the

mass flow of the spike $M_{spike}(t)$, the isotope ratios of the spike R_{spike} and the sample R_{sample} (see

Equation 2) and the isotopic abundances a_i can be considered constant.

$$R_{spike} = \frac{a_{56_{Fe,spike}}}{a_{57_{Fe,spike}}} = 0.03 \text{ and } R_{sample} = R_{nat} = \frac{a_{56_{Fe,nat}}}{a_{57_{Fe,nat}}} = 41.7$$

<center>Equation 2</center>

The isotope ratios of the spike (R_{spike}) and the sample (R_{sample} = R_{nat}) can be calculated from the isotope abundances of ^{56}Fe and ^{57}Fe in the spike (as known from the certification) and the natural abundances.

R_{blend}, the ratio of the mixture of eluent, sample and spike, is calculated by the ratio of the

measured signals of ^{56}Fe and ^{57}Fe at each point in time (Equation 3).

$$R_{blend} = \frac{measured\ signal\ ^{56}Fe}{measured\ signal\ ^{57}Fe}$$

<center>Equation 3</center>
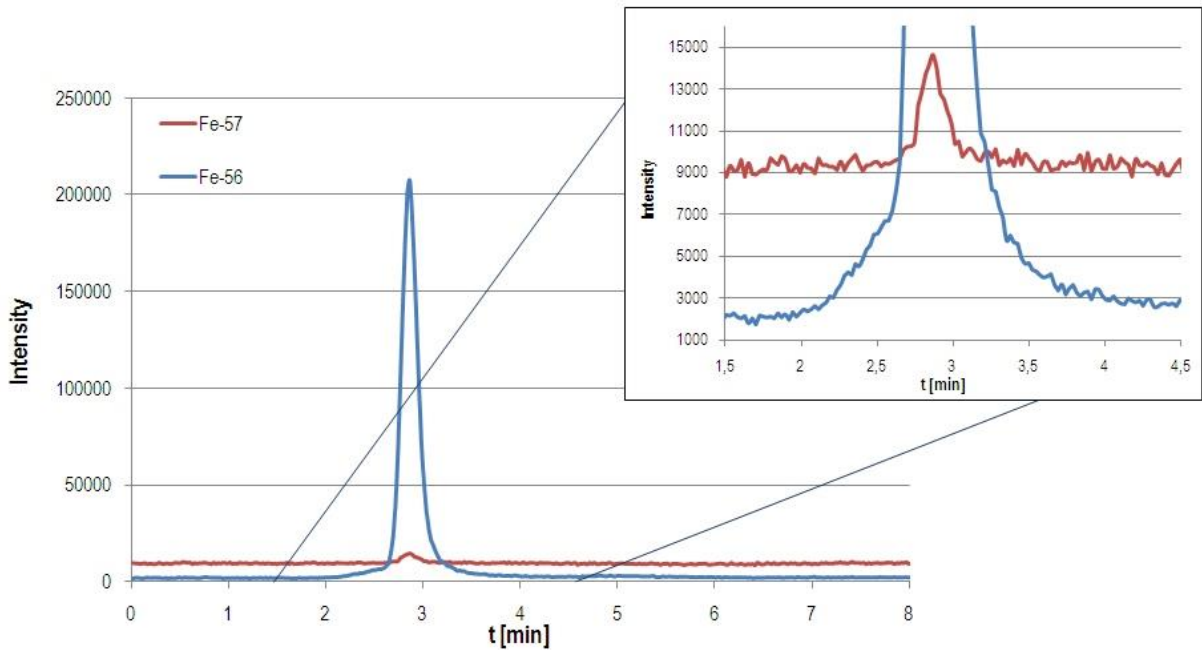

<center>**Figure 9: 10 µM Fe-DMA standard**</center>

Chromatogram showing the change in the ^{56}Fe to ^{57}Fe ratio during the Fe-DMA peak with an ^{57}Fe of 3.3 pmol min^{-1}.

As the iron concentration detected in eluent and spike should be constant, iron in the spike

produces a peak in the mass flow chromatogram (see Figure 10), which when integrated over

time gives the amount of iron (n_{sample}, Equation 4) in the injected sample volume. The iron concentration of the sample c_{sample} can then be calculated by relating the absolute amount to the injected volume $V_{injection}$ (Equation 5).
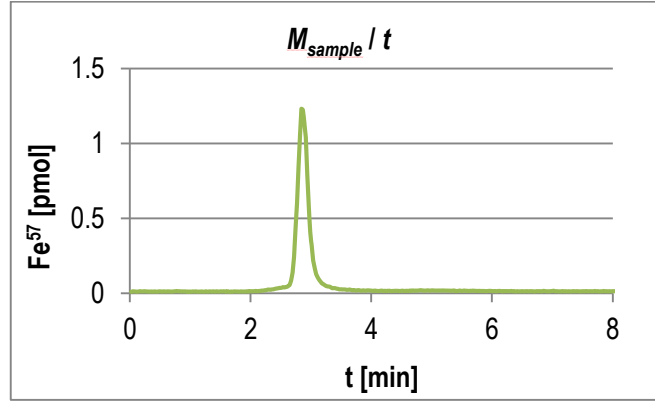

Figure 10: Mass flow chromatogram of Figure 9

Iron mass flow of the measurement shown in Figure 9, calculated via Equation 1 for each point in time. The peak area reveals the amount of iron in the sample n_{sample}.

$$\int_{t_0}^{t} M_{sample}(t) = n_{sample}$$

Equation 4

$$c_{sample} = \frac{n_{sample}}{V_{Injection}}$$

Equation 5

The mass flow was calculated in Microsoft Excel, while the integration of the peaks was done in Microcal Origin 5.0, Microcal Software, Inc., Norhampton, MA 01060 USA.

3. Results and Discussion

The aim of the present work was to develop a quantification method via LC-ICP-MS for metal-DMA complexes in soil matrices. Post column IDMS using stable iron isotopes, external standard calibration, standard addition and comparison with total DMA content analysed via LC-ESI-MS were implemented and evaluated for quantification and quality control.

3.1.   LC-Separation of Metal-Phytosiderophore complexes

As discussed in Chapter 1.3, a mixed mode RP/WAX column was used for the chromatographic separation of the metal phytosiderophore complexes. The functional group of the stationary phase consists of a tertiary amine with a pKa of about 9.9 (N-(10-undecenoyl)-3-aminoquinuclidine selector). As measurements took place at a pH of 6.5, where the PS metal complexes are singly negatively charged, anion exchange with the protonated amine is the main mechanism controlling the separation, while hydrophobic interaction with the carbohydrate chain plays only a minor role. While free metals elute with the void volume, free iron is hardly soluble under neutral conditions. It is therefore accumulated in the system and seen as an elevation of the background. As the measurement takes place in equilibrium between precipitated iron and soluble iron, it is very important that the iron introduced into the system is minimized and the system is well flushed to allow equilibration.

	Fe	Co	Ni	Cu	Zn
RT / min	2.75	2.40	2.57	2.31	1.83

Table 4: Retention times *RT* in minutes of the investigated metal-DMA complexes

As can be seen in Figure 11, metal complexes of all Fe(III), Co(II), Ni(II), Cu(II) and Zn(II) were detected. The respective retention times (*RT*) are shown in Table 4. The dead time t_0 was 0.48 min.
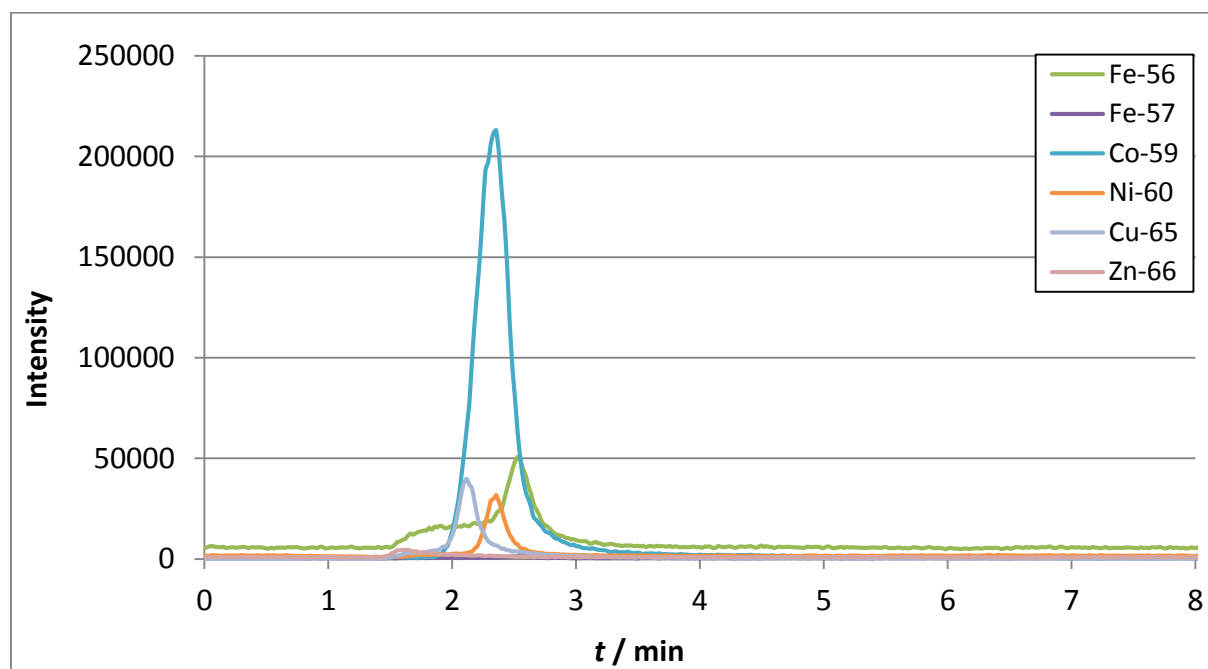

Figure 11: 2.5 µM Metal-DMA Standard

DMA complexes with Fe(III), Co(II), Ni(II), Cu(II) and Zn(II) detected via the metals through the retention of the metal complexes. Separation between the different metal complexes is not needed for identification. The components were separated via a customized RP/WAX column (2.1 x 50 mm PEEK) and the dead time t_0 was 0.48 min.

A major problem when analysing metal-phytosiderophore complexes is that the metal complexes are of course in equilibrium with the free metal in solution, which is in equilibrium with the metal in solid form. Due to the extremely low solubility of iron at a pH of 6.5, neutral aqueous solutions of iron complexes cannot be in equilibrium, as the solid iron is missing. The intensity loss observed when measuring iron-phytosiderophore complexes over time, was therefore explained through disassociation of the complex and precipitation of iron (see Figure 12).
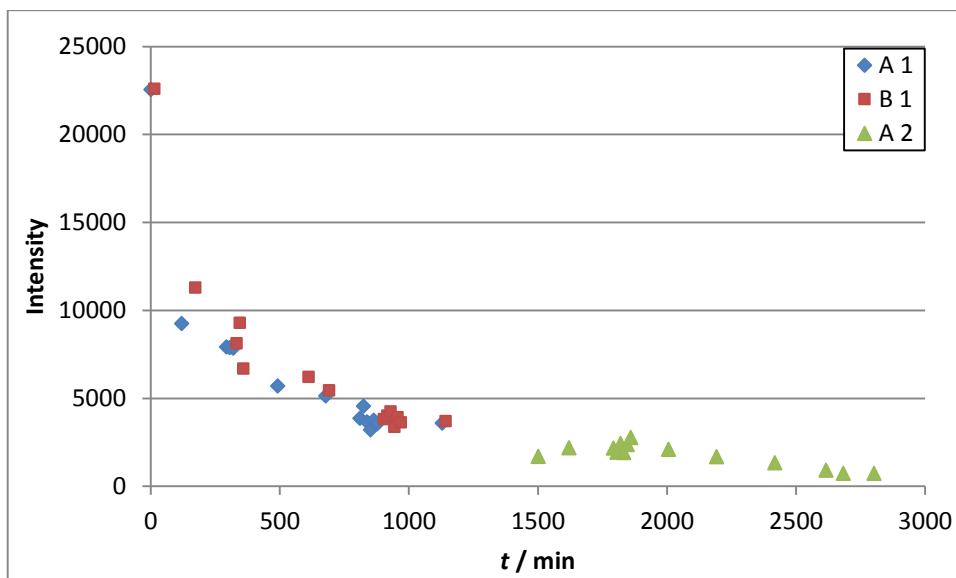
Figure 12: Fe-DMA over time

2 samples of 10 µM Fe-DMA were measured (A1 and B1) over 19 hours. A2 shows sample A1 measured once more a week later, this time over 22 hours. While short term precision was high, the observed intensity loss for Fe-DMA over time prevented high long term precision.
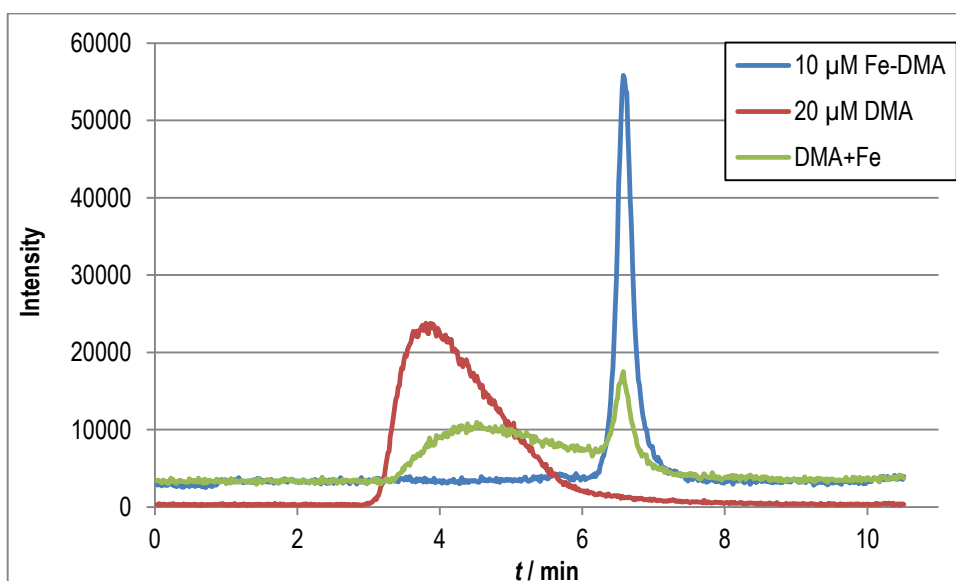

Figure 13: Peak shapes of DMA, Fe-DMA and DMA containing iron

Peaks found when analysing iron-DMA mixtures in different relations. DMA (red) elutes consistently with LC-ESI-MS analyses of DMA and Fe-DMA before the metal complex (blue). Green shows a mixture of iron and DMA with a surplus of DMA.

Due to the disassociation of the metal-phytosiderophore complex, the iron-DMA peak is sometimes found on the shoulder of a very broad peak (Figure 13: DMA + Fe). This also occurs,

when the iron DMA solution contains an excess of DMA. As it is known that DMA elutes before the iron-complex and a measurement of DMA results in a broad tailing peak (Figure 13: 20 μM DMA), it is believed that this broad peak is induced by free DMA collecting iron in the system. Depending on when during the analysis the iron complex was formed, the elution time will be nearer to that of free DMA or of the iron complex.

Figure 14 shows the chromatograms of two samples. At 0.4 min (dead time) the unretained free metals are observed. As iron is hardly soluble at pH 6.5, no free iron is detected under these measuring conditions. The ^{56}Fe and ^{57}Fe peaks, which don't appear in the standard solutions and show an uncommon ^{56}Fe/^{57}Fe ratio, are Ca-oxides (^{40}Ca^{16}O interferes with ^{56}Fe at m/z 56, and ^{40}Ca^{16}O^{1}H interferes with ^{57}Fe at m/z 57). They were also found when a solution of Ca was measured. When using IDMS, this peak did not appear in the mass flow chromatogram.
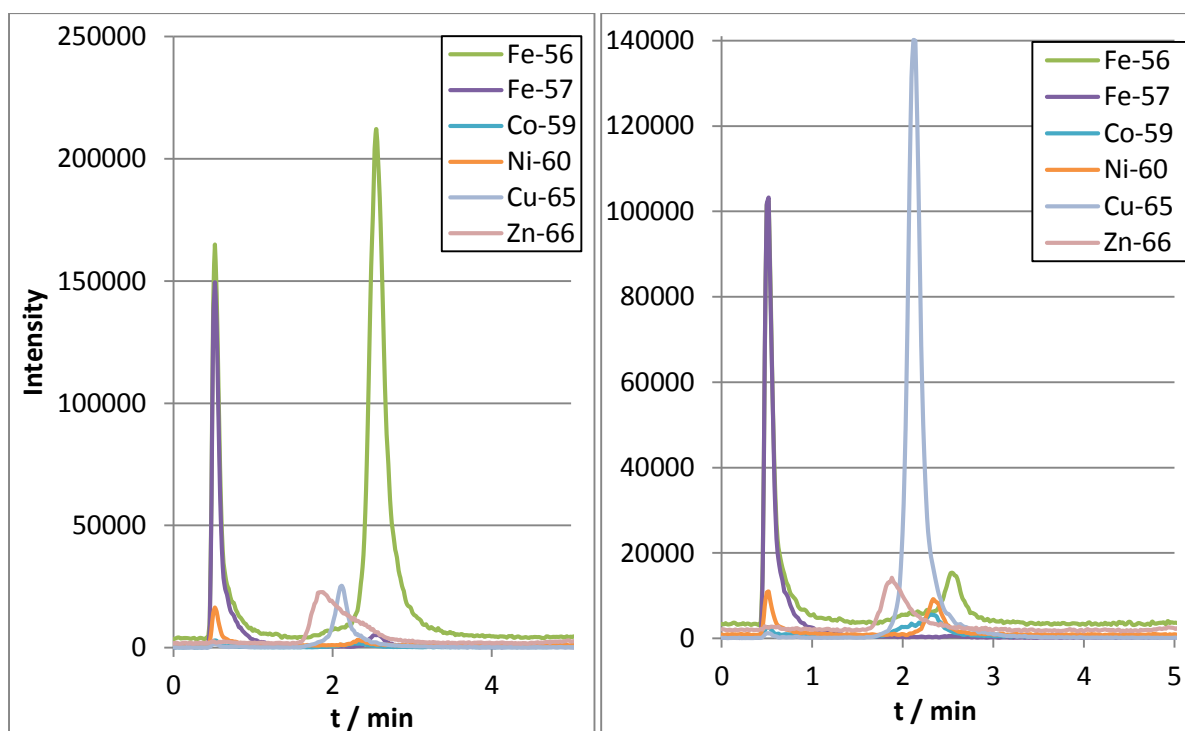

Figure 14: a) Sample P3, b) Sample P7

At 0.4 min (dead time), the unretained free metals arrive, with exception of iron (^{56}Fe as well as ^{57}Fe), as no free iron was detected at pH 6.5. The peak in a signal form CaO (^{40}Ca^{16}O interferes with ^{56}Fe at m/z 56, and ^{40}Ca^{16}O^{1}H interferes with ^{57}Fe at m/z 57), as it is also found when a solution with Ca is measured.

Although iron, cobalt, nickel, copper, and zinc complexes could be detected in the samples, the quantification proved to be challenging – especially for iron and zinc.

Figure 15 shows the measurement of 3 µM metal standards over time. The measured concentrations were calculated via external calibration standards. As can be seen, the fluctuations are vastly different between the different metals. Both iron and zinc possess relative standard deviations (RSD) of over 30 % and the mean value of 9 µM for zinc differs vastly from the prepared control concentration of 3 µM. These inconsistencies are probably due to zinc impurities in the system and are the reason why the low zinc concentrations found in soil related samples were not evaluated.
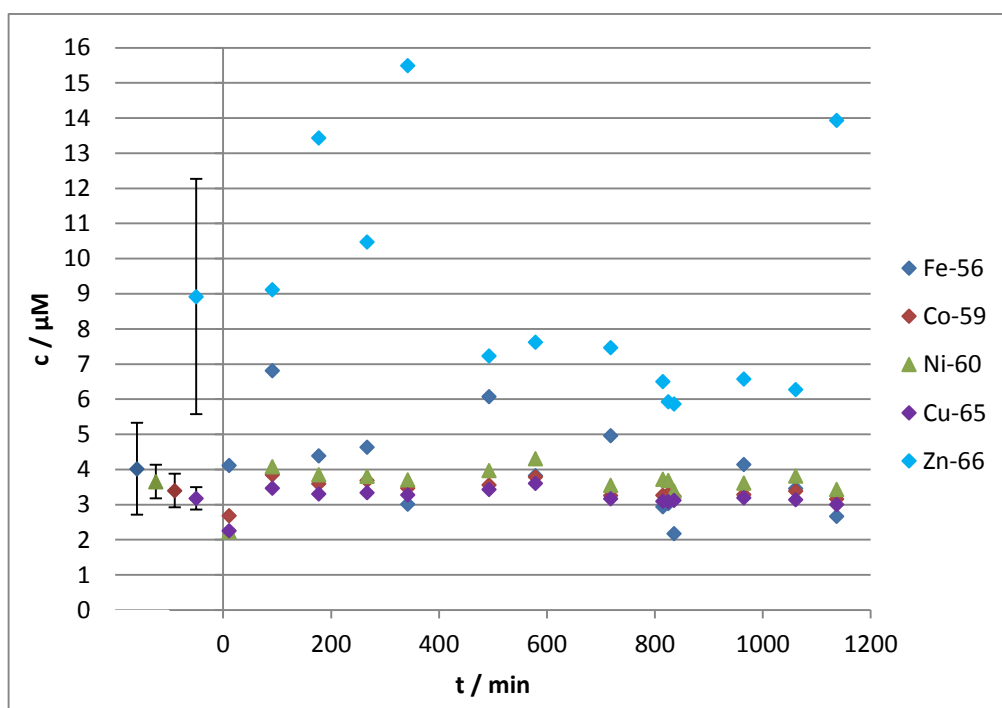

Figure 15: Concentration over time

The concentration of a 3 µM multi-elemental control (c_{Me} = 3 µM for all analysed metals, c_{DMA} = 30 µM) calculated via external calibration over time. On the left side of the diagram, mean values and standard deviations are shown (relative standard deviation were ^{56}Fe 32 %, ^{59}Co 9 %, ^{60}Ni 30 %, ^{65}Cu 10 % and ^{66}Zn 40 %).

While the relative standard deviation of iron is also quite high with 32 %, the 'true value' is within the standard deviation of the mean value (4.0 µM) and the iron-DMA concentrations found in samples were much higher.

The standards for the external calibration were prepared in form of multi-elemental standards, as the sensitivity loss over time demands regular control via standard measurements (calibration and control solutions) as well as a minimisation of the measurement time.

To prevent unnecessary metal-contamination of the system (especially concerning zinc and iron), the concentration ranges were scaled in relation to the amounts expected in the samples ($c_{Fe} = 2\ c_{Cu} = 2\ c_{Zn} = 4\ c_{Co} = 4\ c_{Ni}$). The concentration range for iron was set from 1 to 20 µM, thus resulting in copper and zinc concentrations from 0.5 to 10 µM and cobalt and nickel calibration limits of 0.25 to 5 µM. The scaling also aimed to minimize fluctuations in the iron concentration due to competing metals.

The DMA concentration in multi-elemental standards was adjusted to 1.2 times the total metal concentration (slightly in abundance), as it would be desirable to prevent competition between the metals for complexation with DMA as well as free DMA chelating metal atoms during the measurement and thus creating broad peaks.

LOD/LOQ	Fe-56	Co-59	Ni-60	Cu-65	Zn-66
LOD / µM	0.5	0.003	0.04	0.01	0.08
LOQ / µM	1.5	0.009	0.14	0.03	0.25
$LOD_{abs} = LOD \cdot V_{inj}$/ pmol	2.5	0.015	0.20	0.05	0.40
$LOQ_{abs} = LOQ \cdot V_{inj}$/ pmol	7.5	0.045	0.70	0.15	1.25

Table 5: LODs and LOQs

The Limits of Detection (LODs) and Limits of Quantification (LOQs) for iron and zinc are in the low µM range, for cobalt, nickel and copper in the nM range.

The LODs (limit of detection = 3 σ) and LOQs (limit of quantification = 10 σ) were calculated via the following equation

$$LOD = \frac{6\,\sigma * c}{2\,h_{peak}}$$

Equation 6: Calculation of the limit of detection

The peak height h_{peak} and the noise range $6\,\sigma$ (the difference between the upper and the lower noise level) were determined from chromatograms.

Due to the relatively high backgrounds of iron and zinc – in spite of all measures taken to lower them – the LODs and LOQs of these two metals are in the lower micro-molar range and much higher than those of cobalt, nickel and copper, which are 10, 140 and 30 nM respectively (see Table 5).

Short and long-term precision (see Table 6, Table 7 and Table 8) was high for cobalt and copper, quite good for nickel and worst for iron and zinc (around 20 % relative standard deviation).

short term precision	Fe-56	Co-59	Ni-60	Cu-65	Zn-66
QC (Average, n 3) / μM	2.7	3.27	3.6	3.1	6.1
QC (RSD) / %	17	0.93	5.2	0.56	5.8

Table 6: Me-DMA short term precision (~30 min)

Short term precision of a multi-elemental standard (c_{Me} = 3 μM for all analysed metals, c_{DMA} = 30 μM) calculated via external calibration (see Figure 15).

Due to the loss in sensitivity during the measurement, concentrations $c_{x,lc}$ were calculated via linear combination of the two calibration curves (cal 1 and cal 2) bracketing the sample using the following equation:

$$c_{x,lc} = c_{cal\,1} * \frac{t_2 - t_x}{t_2 - t_1} + c_{cal\,2} * \frac{t_x - t_1}{t_2 - t_1}$$

Equation 7

The mean time of the first and the second calibration (t_1 and t_2) were used to determine the bias for the sample measured at t_x.

As no short term precision experiment with more than 3 consecutive measurements of all metals was measured, Table 7 shows the short and long term precision of Fe-DMA measured with a 100 x 2.1 mm PEEK column with the same stationary phase as the column otherwise used. For this experiment, only iron was examined.

Fe-56	**a)**	**b)**
QC (Average, n 6) / μM	7.3	7.7
QC (RSD) / %	19.1	22

Table 7: Fe-DMA precision a) short term; b) long term

a) **Short term precision (6 consecutive measurements → ~80 min) with 10 μM Fe-DMA;**

b) **Long term precision with 10 μM Fe-DMA over 1300 min within the same measurement (RP/WAX . The sensitivity loss is reduced by calculation of the QC concentration via linear combination between the two regression curves measured before and after the sample.**

	Fe-56	**Co-59**	**Ni-60**	**Cu-65**	**Zn-66**
QC (theoretic) / μM	10	2.5	2.5	5.0	5.0
QC (Average) / μM	8.6	2.45	2.75	5.29	4.25
QC (RSD) / %	18	8.0	12	6.6	12

Table 8: Long term precision (19 h)

Long term precision over 19 h with a multi-elemental standard ($c_{Fe} = 2\ c_{Cu} = 2\ c_{Zn} = 4\ c_{Co} = 4\ c_{Ni}$) with an abundance of DMA ($c_{DMA} = 1,2\ c_{Me,\ tot}$). The sensitivity loss over time is reduced by calculating the concentrations via linear combination between the two regression curves measured before and after the sample using Equation 7.

3.2. Comparison of different quantification strategies

3.2.1. *Quantification via post column IDMS*

Post column IDMS was applied to quantify the iron-phytosiderophore complex via the iron mass flow. As an absolute method, this quantification is independent of fluctuations in the ICP measurement after addition of the spike and could provide a control for the external calibration.
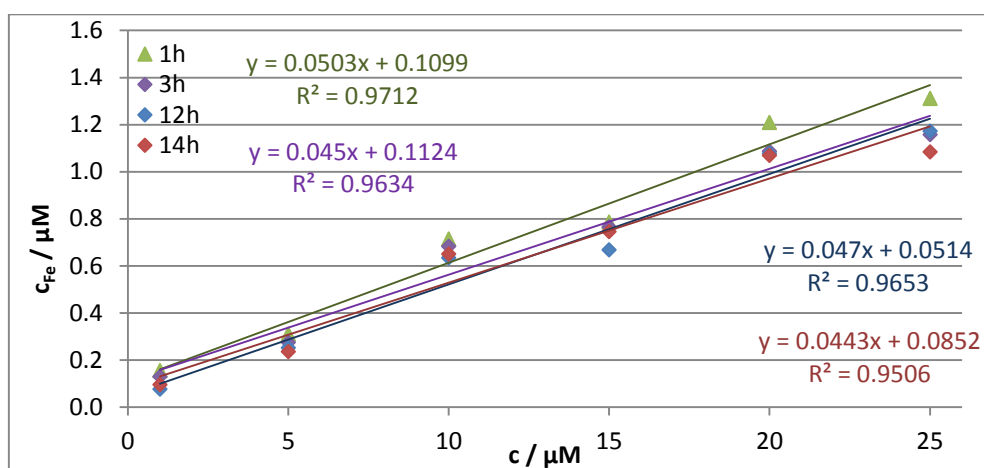

Figure 16: Fe-DMA Calibration calculated via IDMS
The concentrations found by IDMS were much smaller than expected (about 5% of the expected amount). In most cases about 20-30 % of the theoretical concentration were measured (see Figure 17).

Figure 16 shows four measurements of calibration solutions in the range from 1 to 25 μM. As can be seen, the concentrations calculated via IDMS were quite constant, but considerably lower than expected. In Figure 17, the results of quantifications of LC and FIA measurements calculated via IDMS and external calibration for known concentrations can be seen. The theoretical concentrations were plotted against the measured concentration, showing that the absolute iron concentrations calculated via IDMS only reached about 20 to 30 % of the expected concentrations.

These low column recoveries can be explained, when possible iron loss during the separation is considered. As the chromatographic separation takes place at a pH of 6.5 in an environment

containing a minimum of solid iron, it is probable that the complex dissociates followed by iron micro-precipitation. This assumption could be confirmed by a comparison of the slopes of FIA and LC-regression curves (see Table 9). The higher slopes found in the FIA measurement indicate an iron loss during the measurement, thus eliminating the possibility of an absolute quantification of iron in the sample via IDMS.
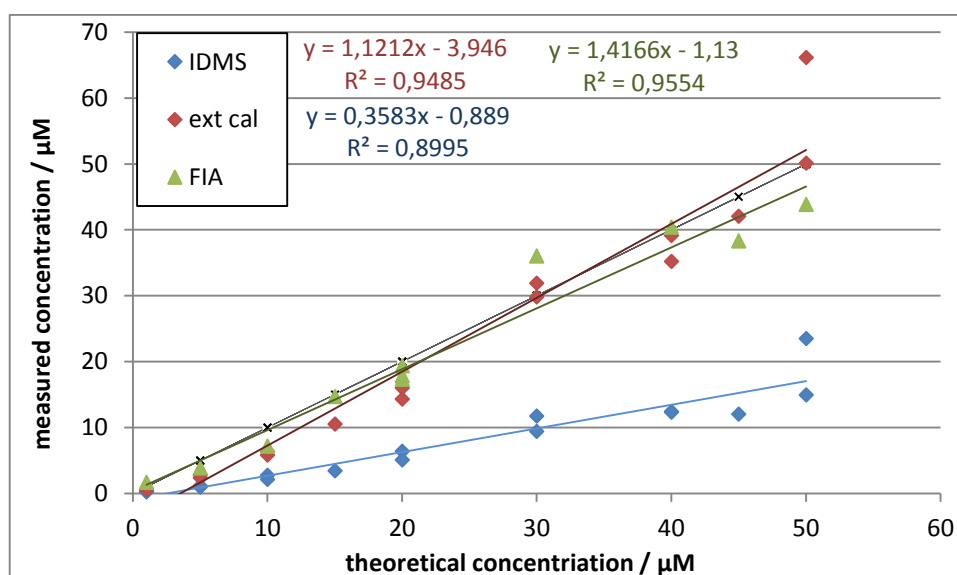

Figure 17: Comparison of different quantification strategies

Iron standards were measured via FIA (green) and LC (blue and red) and calculated via external calibration (green and red) and via IDMS (blue).

As IDMS doesn't correct for losses before the addition of the spike isotope, the results obtained via IDMS are only valid for the concentrations measured in the detector and don't correspond to the concentrations contained in the samples.

Though the addition of ^{57}Fe could not be used for quantification as intended and had the undesirable effect of elevating the iron background, the findings had useful consequences. The post column spike made it possible to observe the stability of the sensitivity of the mass analyser and the fact that is contained a low percentage of HNO_3 minimised further iron losses after the separation through acidification of the system. The post column addition of an acidic solution was therefore continued even when IDMS was not used.

To avoid the higher iron back ground, it was tried to exchange iron with indium in 2 % HNO₃, but intensity changes in iron and indium over time were not comparable, making a slight elevation in the iron background seem preferable.

While the acidification of the system is beneficial, as it prevents further iron loss, it is impossible to implement before or during the chromatographic separation, where a neutral pH is needed for the separation as well as complex stability.

3.2.2. *Quantification via external calibration*

As IDMS could not be used for sample quantification due to metal losses prior to the addition of the internal standard (see Chapter 3.2.1), samples were analysed via external calibration.
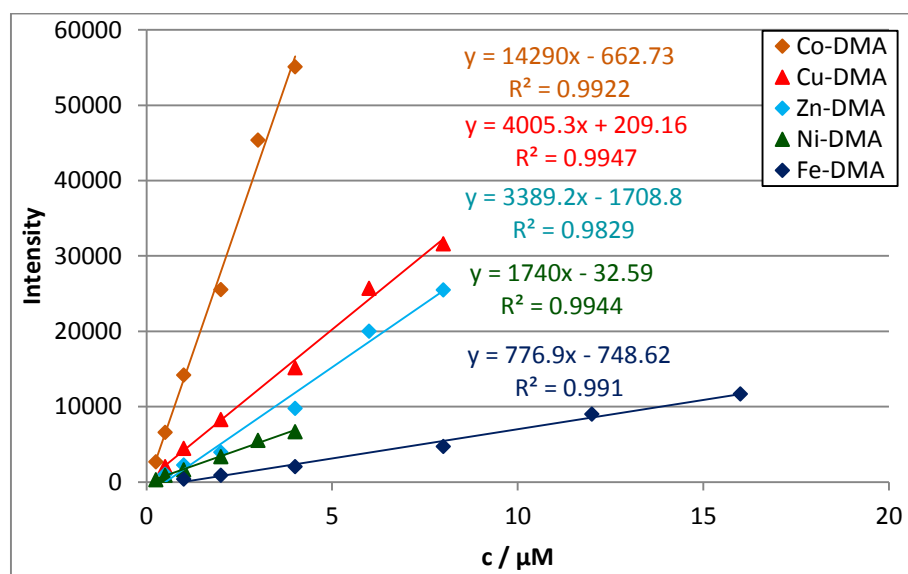

Figure 18: External calibration curves for LC

6 point calibration for iron (1 to 16 µM), copper, zinc (0.5 to 8 µM), cobalt and nickel (0.25 to 4 µM) measured via liquid chromatography.

Species specific metal-DMA standards prepared the day of the measurement in a concentration range of 0.25 to 20 µM were used to calculate sample concentrations over linear regression

curves (see Figure 18). Control standards and standard addition were used to assess if there were deviations over time or due to sample matrix effects (see Chapter 3.2.3).

Due to the observed loss in sensitivity over time (see Chapter 3.1), linear combination between the two calibration curves bracketing the samples were used to derive the sample concentrations (see Equation 7).

	k_{FIA}	k_{LC}	k_{LC}/k_{FIA} / %
Fe	3146	405	13
Co	10444	13083	125
Ni	2388	1987	83
Cu	3157	3423	108
Zn	1737	261	15

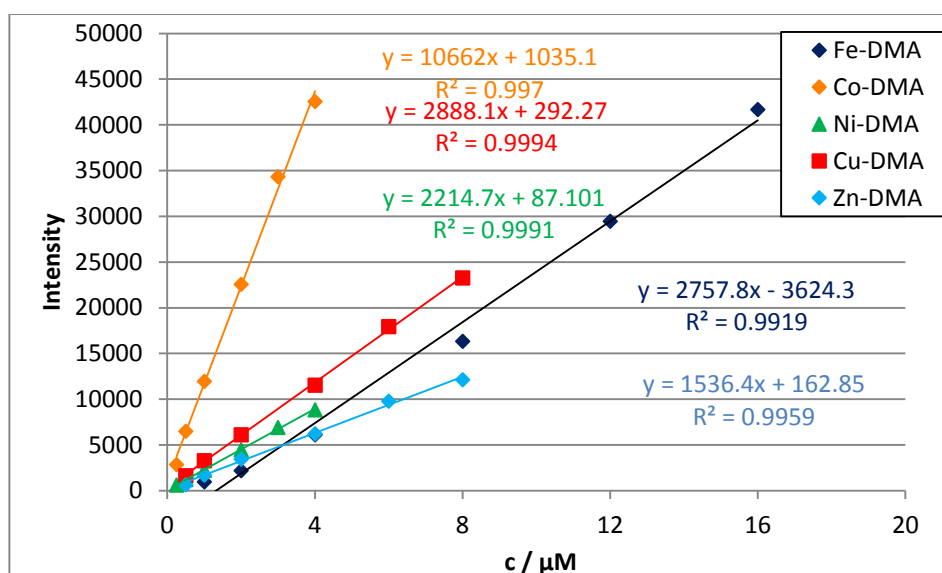**Table 9: Comparison of LC and FIA slopes**

Figure 19: External quantification for FIA

6 point calibration for iron (1 to 16 μM), copper, zinc (0.5 to 8 μM), cobalt and nickel (0.25 to 4 μM) measured via flow injection analysis (FIA).

Figure 19 shows the same solutions measured via flow injection analysis (FIA). As can be seen, the slopes of the FIA measurement are much steeper than those found via LC (see Table 9). While the response of the mass analyzer and the metal solubility are responsible for slope differences for the various elements, the high differences between FIA and LC point to low

column recovery due to losses of the DMA-metal complexes during the LC measurement, as already discussed above.

3.2.3. Quantification via standard addition

Quantification via standard addition was implemented on a few randomly selected samples to assess possible influences of the sample matrices. From samples chosen for standard addition six aliquots were prepared for the measurement. While only water was added to the first, metal-DMA standards in the concentration scaling, also used for calibration ($c_{Fe} = 2\ c_{Zn} = 2\ c_{Cu} = 4\ c_{Ni} = 4\ c_{Co}$), were added to the other aliquots.
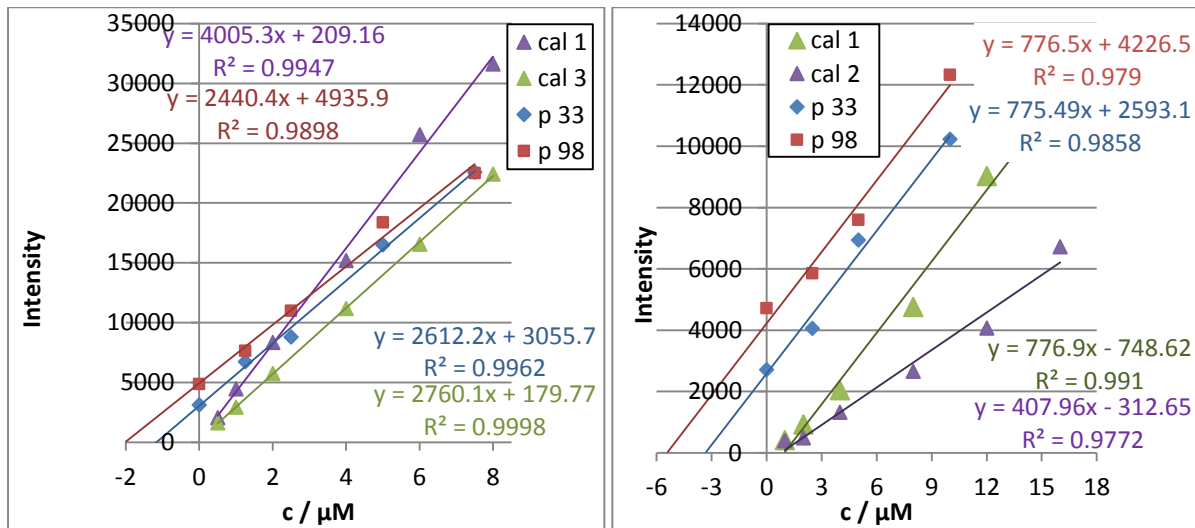

Figure 20: Regression curve for the standard addition and calibration of a) Cu-DMA and b) Fe-DMA

The slopes of the regression curves of Metal-DMA of two calibration curves (cal 1, cal 2, cal 3) and standard addition to different samples (p 33 and p 98) compare quite well. The results obtained are compared in Table 10. In Figure 21, the slopes depicted here are correlated with the time of the measurement.

The concentrations were calculated via the regression curve ($c_{St-Add} = -x_{y=0} = \frac{d}{k}$), which is the intersection between the regression curve of the standard addition and the x-axes (Figure 20). As the results obtained from soil samples had a high variation (see Table 10 and Chapter 3.3) – partly due to the intensity change over time – the slopes of the external calibration and

33

standard addition were compared. In the following, an objective comparison of the slopes and therefore a possible influence of the matrix on the regression slopes is attempted.

While the slopes of the regression and calibration curves shown in Figure 20 compare quite well, it is difficult to evaluate observed differences. Figure 21 shows the slopes of the calibrations ($k_{Me} = \frac{(y-d)}{x}$) and standard additions k_{Me} (p33 or p98) over time. The decrease of the slope over time is evident, especially for cobalt, copper and zinc. It is also apparent, that the regression curves of the calibrations for cobalt and copper are slightly steeper than the corresponding standard addition curves, while iron and nickel show an adverse effect.
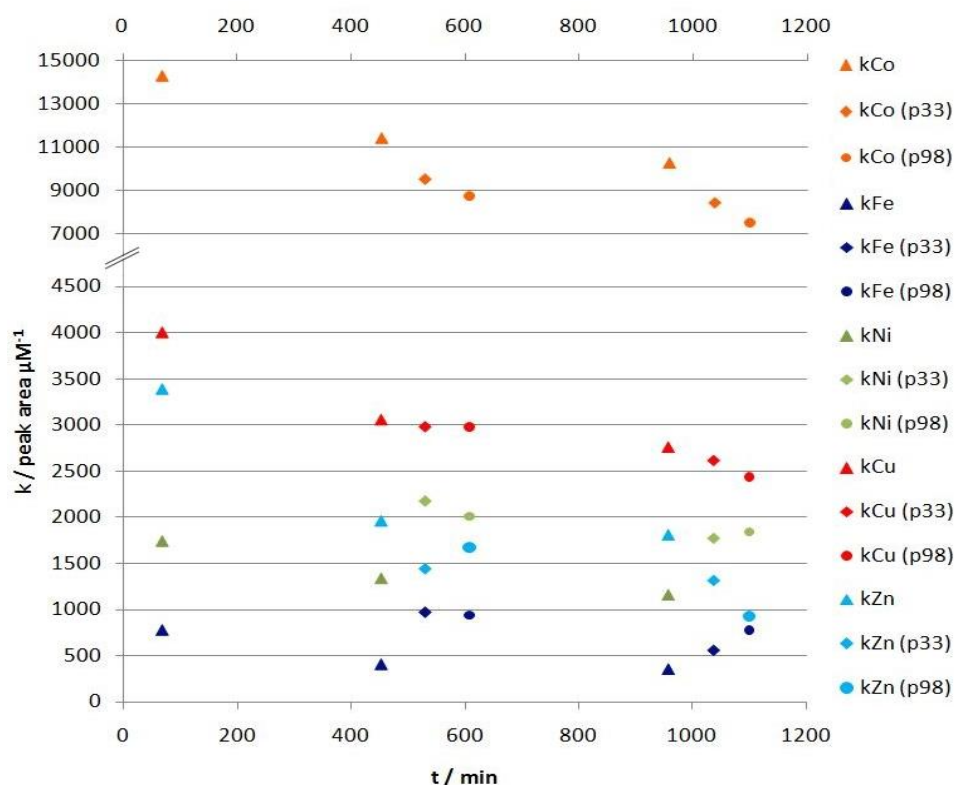

Figure 21: Slopes over time

The slopes of the calibrations ▲, of standard addition in sample p33♦, and in sample p98 ● are shown for Fe(III), Ni(II), Cu(II) and Zn(II), as well as Co(II), which has much steeper slopes in a range from 7500 to over 14 000 peak area/µM. The flattening of the slope over time is obvious, especially for Cu(II), Zn(II) and Co(II). The diagram also shows, that the standard addition slopes for iron and nickel are a bit higher than their calibration slopes while those of copper are a bit lower than the respective calibration.

While this could be a matrix effect, it is more likely that the ratio of the metal concentrations in the individual solutions is responsible, highlighting one of the major problems when analysing complexes with competitive metals of unknown and varying concentrations in equilibrium with each other.

In order to see if the metal concentrations could be responsible for the shifts, the metal concentrations in the calibration solutions and in the samples have to be compared. The measured data are shown in Table 10. Although the relative standard deviations (RSD) for iron and zinc are very high (around 50 %), it is still obvious that the samples contained hardly any cobalt and nickel, while some iron, zinc and a little copper were found. The metal ratio in the calibration solution was set to $c_{Fe} = 2\ c_{Zn} = 2\ c_{Cu} = 4\ c_{Ni} = 4\ c_{Co}$, the ratio found in the sample is approximately $c_{Fe} = 2\ c_{Zn} = 5\ c_{Cu} = 20\ c_{Ni} = 116\ c_{Co}$.

		Fe		Co		Ni		Cu		Zn	
		$c_{St\text{-}Add}$	$c_{ext\ cal}$	$c_{St\text{-}Add}$	$c_{ext\ cal}$	$c_{St\text{-}Add}$	$c_{ext\ cal}$	$c_{St\text{-}Add}$	$c_{ext\ cal}$	$c_{St\text{-}Add}$	$c_{ext\ cal}$
p33	1	1.86	6.90	< LOQ	0.06	0.05	< LOQ	0,99	1,20	4,62	3,70
	2	5.86	8.10	< LOQ	0.03	0.58	< LOQ	1,17	1,10	4,21	3,20
p98	1	3.52	11.10	< LOQ	0.08	0.36	0,39	1,67	1,70	2,85	2,50
	2	5.44	13.70	0.12	0.04	0.27	0,34	2,02	1,70	5,38	2,60

Table 10: Results via external calibration and Standard Addition

Concentrations measured via LC in µM (sample dilution 1:4). Iron and zinc have a relative standard deviation (RSD) of about 50 %, the other metals compare very well; the high standard deviation found in the case of cobalt is due to the low concentration (LOQ of 0.01 µM).

To evaluate if the observed shifts are significant, Figure 22 once again illustrates the slopes of the calibration and the standard addition curves in order to compare the mean values and

standard deviations. This arrangement shows that with the exception of cobalt, the shifts are within the standard deviation caused by the slope decrease over time. The results led to two conclusions: (1) the sensitivity of the investigated elements is related to column recovery, isotope abundance and direct ICP-MS sensitivity (e.g. ionisation potential) (2) the complexes are not stable over time – stabilisation needs to be optimised testing different buffer solutions and pH ranges.
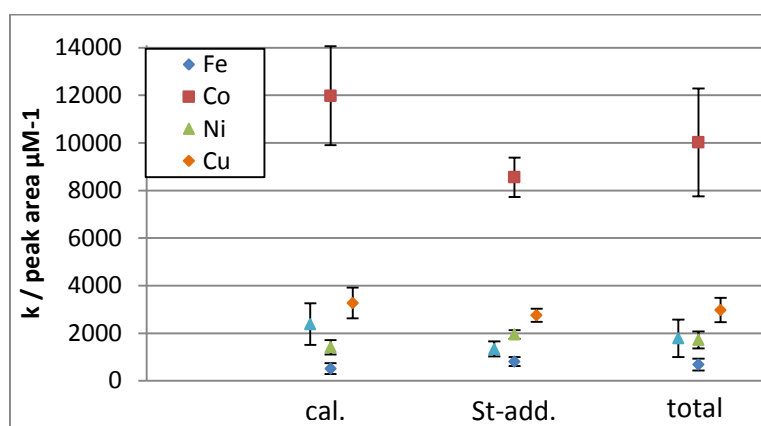

Figure 22: Matrix effects on regression curve slopes

The slopes of three measurements of a calibration solution over 16 hours (cal.; n 3) compared to the slopes of two standard additions each measured twice (St-add.; n 4). With the exception of Co-DMA, the changes are within the standard deviation caused by the slope decrease over time. Total shows the slopes and standard deviations of the combined regression curves for the five metal-DMA complexes.

3.3.   Analysis of soil samples

While possible matrix effects have been discussed in connection with standard addition (see Chapter 3.2.3), results from the comparison of LC and flow injection analysis (FIA) data are discussed in the following chapter.

Figure 23 shows a comparison between the concentrations of iron (blue via FIA-ICP-MS, and red, measured by the Department of Environmental Geosciences from the University of Vienna), the total DMA (green via LC-ESI-MS/MS) and the Fe-DMA complex (violet via LC-ICP-MS) shows that the results compare quite well. The two ICP measurements show very similar results (with the exception of sample 13), but it is interesting to see that the

concentrations measured via FIA-ICP-MS are generally lower than those found via LC-ICP-MS.
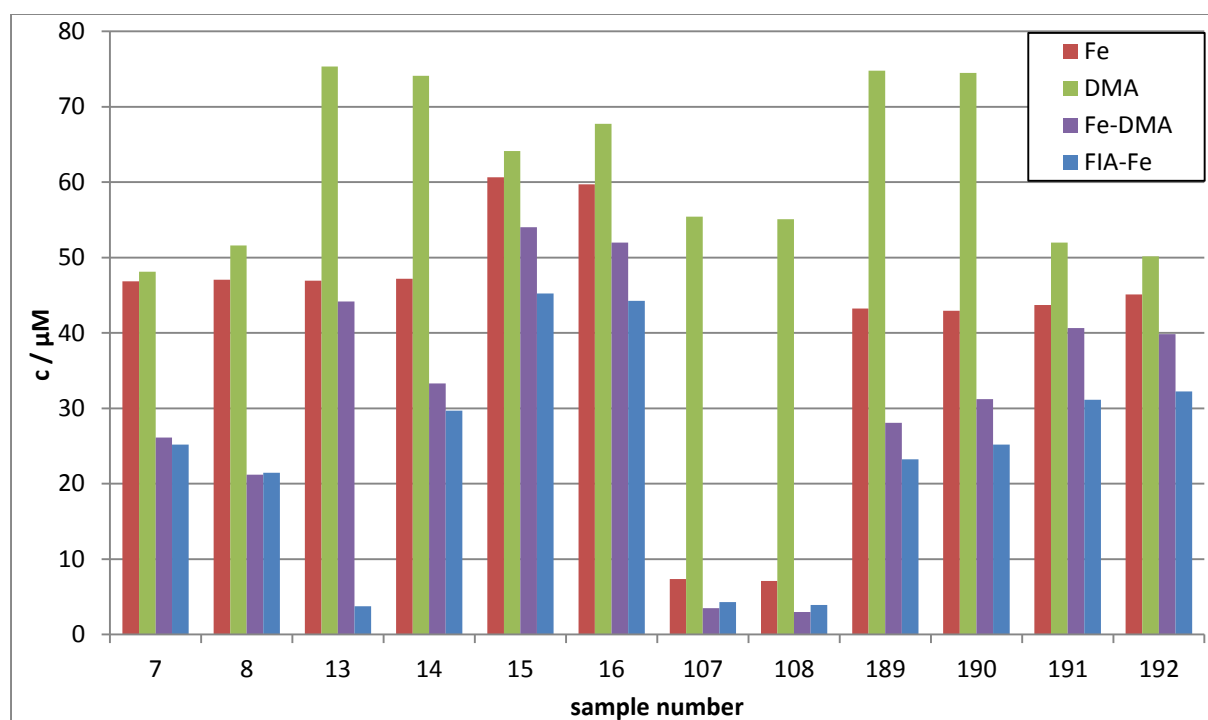

Figure 23: Iron-DMA content of selected soil samples

A comparison between the concentrations of iron (blue via FIA-ICP-MS, and red, measured by the Department of Environmental Geosciences from the University of Vienna), the total DMA (green via LC-ESI-MS/MS) and the Fe-DMA complex (violet via LC-ICP-MS) shows that the results compare quite well. The two ICP measurements show very similar results (with the exception of sample 13), but it is interesting to see that the concentrations measured via FIA-ICP-MS are generally lower than those found via LC-ICP-MS.

Figure 24 shows a comparison between the metal-DMA complex (excepting zinc) and the total DMA and metal concentrations. The results compare quite well for most soil samples, especially the samples 2 to 90. Samples containing azide (N_3^-, sample names with N3) show less compatibility. In the samples 114, 146, 161 metal-DMA concentrations were below the limit of quantification, fitting with the low total DMA concentrations found in these samples. Interestingly, the samples 122, 153, 170, 185, 33, and 98 have total DMA concentrations similar to the samples between 2 and 90, but the metal-DMA concentrations found were much higher. While the concentrations are still in a range that is theoretically possible, as the soils were treated with 100 µM DMA, the complex concentrations should be lower than the total DMA

content of the sample. Interestingly the FIA and LC data fit very well excepting the samples containing azide, with very low concentrations and sample 33, which was one of the two samples used for standard addition. The second one, sample number 98, was only measured via LC-ICP-MS. The difference between the two measurements for the samples with low concentrations could perhaps be explained through a higher influence of background concentrations in the FIA measurements, as the FIA concentrations had to be blank corrected, which was not necessary for the LC results.
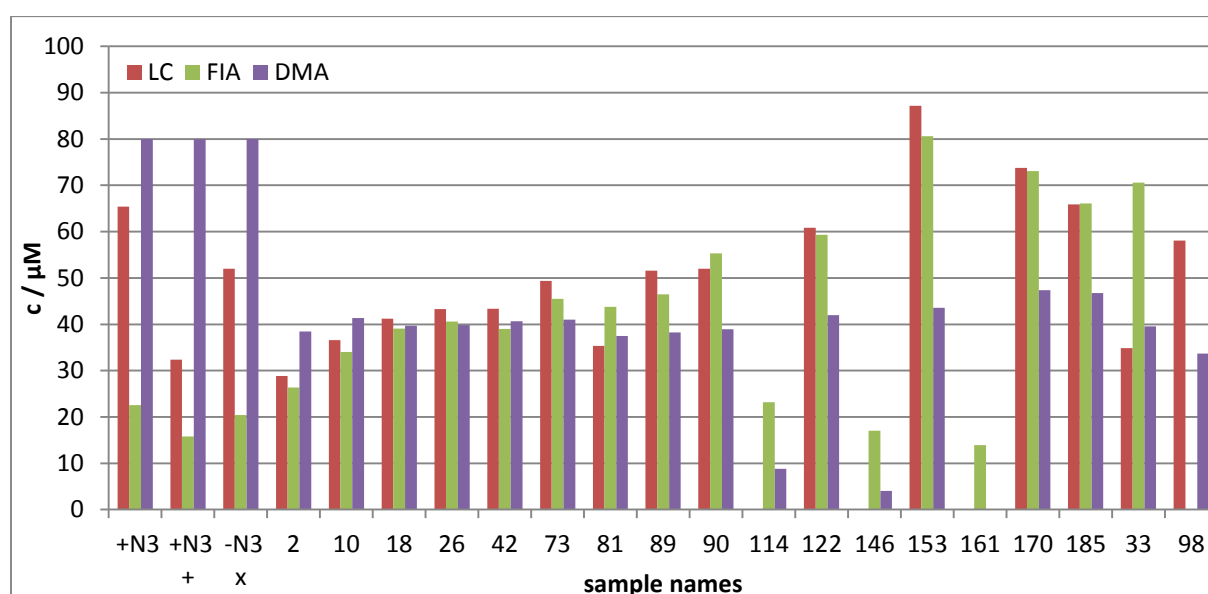
Figure 24: Soil sample results

Comparison between the DMA content (violet), total metal concentrations (green, FIA-ICP-MS) and the total metal-DMA complexes (red, LC-ICP-MS) calculated from the FIA and LC results for the five metals.

An additional control through separate measurement of total metal concentrations via ICP-SFMS was not successful, as the metal concentrations were not reproducible in not acidified solutions (as necessary for the LC-measurement).

Therefore, a comparison with the metal concentrations in the samples is only possible for selected samples, where data measured by the Department of Environmental Geosciences from the University of Vienna were available.

4. Conclusion

Analysis of Metal-DMA complexes poses many challenges, as it means working with different substances whose equilibria depend on the system and on each other. To be able to achieve consistent results, it is therefore necessary to understand these dependencies and to improve the stability and repeatability of the optimised experimental conditions.

Especially iron as an ubiquitous element requires a clean environment and sample preparation to avoid contamination. Further, the iron complex is used to mobilize iron from alkali soils and for that reason is most stable under alkali conditions, where iron is hardly soluble. Under these conditions, iron can easily be lost due to (micro) precipitation, leading to a loss of Metal-DMA. Under more acidic conditions, the Fe-DMA complex was not found, which was explained by dissociation, as it could be observed in the LC-ESI-MS measurement that a measurement of total DMA is possible under acidic conditions.

But as copper and nickel DMA complexes were still found at a pH of 4.75, it is possible that the neutral Fe-DMA complex observed by von Wirén et al.[6] at pH <6 is partly responsible that no Fe-DMA complex was found under mild acidic conditions.

It could be shown through standard addition that the effect of the matrices of the soil samples on the slopes is negligible – especially if compared to uncertainty introduced by stability problems. The observed loss in Fe-DMA intensity was best explained by micro precipitation.

The strong variations found in the results can partly be explained by the changes observed over time and the competing metals, whose concentrations are defined by their content in the sample as well as by impurities in the eluent used. Without assessment of accuracy through complementary (quantification) methods, external standard calibration and a comparison with total DMA contents measured via LC-ESI-MS provided the only means for quantification. The

LC-ICP-MS data presented in this thesis should therefore only be taken as semi-quantitative results.

In spite of these problems, this thesis hopefully helps in expanding our knowledge of the properties of DMA.

Further investigation should be directed in understanding the influences responsible for the changes in intensity and in finding an appropriate control for the presented method, thus ensuring the use of its advantages, e.g. the simultaneous analysis of different Metal-DMA-complexes, which can elute at the same time.

As Xuan et al. stated in 2007, the biggest problem in nearly all published analytical methods for trace metal speciation is not the detection, but the unknown stability of the metal species with respect to the (LC) separation. Even for PS species, that are thermodynamically very stable, partial dissociation may happen in the sample prior to analysis and on chromatographic columns.[19]

5. Appendices

5.1.   Abstract

In case of iron insufficiency "Strategy II"-plants synthesize and exude phytosiderophores (PS), organic ligands able to form soluble iron(III) complexes. The iron can then be resorbed in form of the metal complex via special transporters.

Though phytosiderophores are studied since more than 30 years, little is known about phytosiderophore concentrations in the rhizosphere. This thesis is part of the FWF project "*The rhizosphere biogeochemistry of phytosiderophores and plant iron uptake*" between several divisions of BOKU - University of Natural Resources and Life Sciences and the University of Vienna. The aim of my master thesis in the Division of Analytical Chemistry was to develop methods to quantify metal-phytosiderophore-complexes (primarily iron) via LC-ICP-MS using a stable iron isotope (Fe-57) as species unspecific on line-IDMS-standard.

Extracts from soil samples treated with 2'-deoxymugineic acid (DMA) were analysed to ensure the method's compatibility with soil matrices. As metal-phytosiderophore complexes of Co, Cu, Ni and Zn were detected additionally to Fe(III) complexes, they were implemented into the analytical method.

While an accurate quantitative measurement was not possible as no reliable control could be applied, a semi-quantitative analysis as well as a comparison of the results between the different metal complexes and their behavior in soil and during the analysis was possible.

5.2.   Zusammenfassung

Bei Eisenmangel synthetisieren "Strategie II"-Pflanzen Phytosiderophore (PS), das sind organische Liganden mit der Fähigkeit, lösliche Eisen(III)-Komplexe zu bilden, und geben diese in den Boden ab. Das Eisen kann dann in Form dieser Metallkomplexe über spezielle Transporter aufgenommen werden.

Obwohl Phytosiderophore seit über 30 Jahren erforscht werden, ist nur wenig über ihr Verhalten in der Rhizosphäre bekannt. Die vorliegende Arbeit wurde im Rahmen des FWF Projektes „*Die Biogeochemie der Phytosiderophore in der Rhizosphäre*" in der Abteilung für Analytische Chemie auf der Universität für Bodenkultur Wien in Zusammenarbeit mit Assoc. Prof. Dr. Stephan Hann durchgeführt. Das Ziel der Arbeit ist es, eine LC-ICP-MS Methode zur Quantifizierung von Metall-Phytosiderophor Komplexen mit Schwerpunkt auf Eisen zu untersuchen und ihre Anwendbarkeit auf Bodenproben zu testen. Zur Quantifizierung wird neben externen Standards eine Isotopenverdünnungsmethode mit Fe-57 zur Überprüfung der Messergebnisse herangezogen.

Neben den Fe(III)-Komplexen wurden in mit 2-Desoxymugineinsäure (DMA) behandelten Bodenproben Metall-Phytosiderophor-Komplexe mit Co, Cu, Ni und Zn vorgefunden und daher in die Messmethode mit eingebunden.

Während eine genaue quantitative Analyse auf Grund fehlender zuverlässiger Kontrollmöglichkeiten nicht möglich war, konnten interessante semi-quantitative Untersuchungen zu den unterschiedlichen Metall-Phytosiderophor-Komplexen durchgeführt und ihr Verhalten näher untersucht werden.

5.3. Abbreviations

Ac	acetate
c	concentration
DMA	2'-deoxymugineic acid
ESI	electrospray ionisation
FIA	flow injection analysis
HMA	hydroxymugineic acid
HNO_3	nitric acid
HPLC	high pressure/performance liquid chromatography
ICP	inductively coupled plasma
ID-MS	isotope dilution mass spectrometry
LC	liquid chromatography
LOD	limit of detection
LOQ	limit of quantification
MAs	mugineic acids
MA	mugineic acid
mM	millimol per liter
MS	mass spectrometry
NH_4Ac	ammonium acetate
PEEK	polyether ether ketone
PFA	perfluoroalkoxy
PS	phytosiderophore(s)
RP-WAX	reversed phase/weak anion exchange

RSD   relative standard deviation

RT   retention time

5.4.   Figures

All figures with the exception of Figure 1 (STRUCTURAL FORMULA BY MURAKAMI ET AL. 1989)[4], Figure 2 (a derivative of Figure 1), Figure 3 (STRUCTURAL FORMULA BY SUGIURA AND NOMOTO 1984)[2], and Figure 5 (STRUCTURAL FORMULA BY NOGUEIRA ET AL. 2005)[16], were created by myself.

5.5.   Tables

5.6.   Curriculum Vitae

Personal Information:

Name: REGELSBERGER Anna

Nationality: Austria

Date of Birth: 1986

Education:

present	**University of Vienna** Master degree program Chemistry
2010	**University of Vienna** Bachelor of Science Bachelor thesis: *Stabilitätsuntersuchungen und Zink-Extraktionen mit Polyvinylchlorid-Trihexyltetradecylphosphoniumchlorid-Membranen*, supervised by ao. Univ.-Prof. Mag. Dr. Regina Krachler, Department of Inorganic Chemistry, University of Vienna
2005	**BG/BRG Gleisdorf** (Gymnasium) Matura in June 2005

Publications:

D. Kogelnig, A. Regelsberger, A. Stojanovic, F. Jirsa, R. Krachler, B.K. Keppler. *Monatshefte für Chemie* 142(8) 769-772 (2011)

---

6. Literature

[1] Wallace et al, *Am. Soc. Hort.* 75, 819 (1960)

[2] Y. Sugiura, K. Nomoto, *Struct Bonding*, 58 (1984)

[3] S.M. Kraemer, D.E. Crowley, R. Kretzschmar, *Adv. Agron.*, 91 (2006)

[4] T. Murakami, K. Ise, M. Hayakawa, S. Kamei, S. I. Takagi, *Chem. Lett.* 2137-2140 (1989)

[5] G. Neumann, V. Römheld, R. Pinton, Z. Varanini, P. Nannipier, *The Rhizosphere: Biochemistry and Organic Substances at the Soil-Plant Interface*, CRC Press 2007

[6] N. von Wirén, H. Khodr, R. C. Hider, *Plant Physiol.,* 124 (2000)

[7] G. Weber, G. Neumann, C. Haake, V. Römheld, *Anal. Bioanal. Chem.,* 373 (2002)

[8] G. Weber, G. Neumann, C. Haake, V. Römheld, *J. Chromatrogr. A*, 928 (2001)

[9] S. Kawai, Y. Sato, s. Takagi, K. Nomoto, *J. Chromatrogr. A*, 391 (1987)

[10] D. Schaumlöffel, L. Querdane, B. Bouyssiere, R. Lobinski, *J. Anal. At. Spectrom.*, 18 (2003)

[11] V. Vacchina, S. Mari, P. Czernic, L. Marques, K. Pianelli, D. Schaumloffel, M. Lebrun, R. Lobinski, *Anal. Chem.*, 75 (2003)

[12] Y. Schindlegger, E. Oburger, B. Gruber, W. Schenkeveld, S. Kraemer, M. Puschenreiter, G. Koellensperger, S. Hann, *Electrophoresis*, 35 (2014)

[13] M. Dell'mour, G. Köllensperger, J.P. Quirino, P.R. Haddad, C. Stanetty, E. Oburger, M. Puschenreiter, S. Hann, *Electrophoresis*, 31 (2010)

[14] M. Dell'mour, W. Schenkeveld, E. Oburger, L. Fischerl, S. Kraemer, M. Puschenreiter, M. Lämmerhofer, G. Koellensperger, S. Hann, *Electrophoresis*, 33 (2012)

[15] R. Thomas, *Spectroscopy* 16(10) (2001)

[16] R. Nogueira, M. Lämmerhofer, W. Lindner, *J. Chromatogr. A*, 1089 (2005)

[17] G. Köllensperger, S. Hann, J. Nurmi, T. Prohaska, G. Stingeder, *J. Anal. At. Spectrom.*, 18 (2003)

[18] S.M. Nelms: *ICP Mass Spectrometry Handbook*, Blackwell, Oxford 2005 (ISBN 1-4051-0916-5)

[19] Y. Xuan, E.B. Scheuermann, A.R. Meda, P. Jacob, N. von Wirén, G. Weber, *Electrophoresis,* 28 (2007)